PAPER

Check for updates

Smart electrochromic supercapacitors based on highly stable transparent conductive graphene/CuS network electrodes†

Peijian Yao, ‡[a] Shuyao Xie,‡[a] Meidan Ye, [a] Rui Yu,[a] Qian Liu,[a] Dandan Yan,[a] Weiwei Cai,[a] Wenxi Guo *[a] and Xiang Yang Liu*[ab]

A well-designed flexible ITO-free electrochromic supercapacitor was obtained using a hybrid graphene/ CuS network on PET (G–CuS) as the transparent conductive electrode (TCE). This new type of TCE was produced by photolithography, chemical vapor deposition and a low temperature solvothermal reaction. The TCE achieves a sheet resistance (R_s) as low as ~20 Ω sq^{-1} with a high transmittance of over 85%. In particular, the G–CuS TCE displays a remarkable flexible stability under bending stresses and an excellent chemical stability through the polyaniline (PANI) electrodeposition in acid solution. The PANI/G–CuS electrode gave a favorable area capacitance of 17.3 mF cm^{-2} at 0.025 mA cm^{-2} along with a large optical modulation of 40.1% (620 nm). More intuitively, a symmetrical supercapacitor of PANI/G–CuS was fabricated with H$_2$SO$_4$–PVA hydrogel as the electrolyte, and its noticeable color variation enables users to evaluate the level of stored energy by the naked eye in a predictable manner. This work may provide a practical route to the fabrication of stable TCEs in smart supercapacitors.

Introduction

Supercapacitors are promising electrochemical energy storage devices.[1–3] In recent years, the multifunctional electrochromic energy storage systems have been of increasing interest for the simultaneous realization of energy storage and a smart energy monitor.[4–7] Moreover, the portable, stretchable and flexible features extend their application range.[8–10] Due to the electrochromic property, the transparent conductive electrode (TCE) is a key component of the electrochromic supercapacitor. A TCE typically consists of one or more conductive materials and a transparent substrate such as glass, polyethylene terephthalate (PET) or polydimethylsiloxane (PDMS). In the large family of conductive materials of TCEs, there are tin doped indium oxide (ITO) and various ITO-alternatives including carbon nanotubes (CNTs),[11,12] graphene,[13,14] metal networks,[15,16] poly(3,4-ethylenedioxythiophene)-poly(styrene sulfonate) (PEDOT:PSS)[17,18] and their hybrid materials.[19–21]

Transition metal compounds, like metal sulfides,[22,23] metal nitrides[24,25] and metal phosphides,[26–28] are promising materials

with desired properties for applications in supercapacitors, lithium ion batteries, electrocatalysis, *etc.* Copper sulfide (CuS), one member of the metal sulfide family, is a well-known narrow-band-gap (~2.0 eV) p-type conducting material, which has been reported by several works through directly sputtering CuS film on glass.[29–32] Due to the existence of inherent trade-off between sheet resistance (R_s) and transparency of CuS films, only 60% transmittance was achieved for a 50 nm thickness of CuS film according to the calculation,[30] and further enhancing the transmittance results in a thinner CuS layer which leads to very high R_s. Despite different techniques including chemical and physical approaches have been employed to improve the quality of the CuS films, their optoelectronic performance is still poor with an optimized R_s of ~100 Ω sq^{-1} at ~75% transmittance as reported by Yuan *et al.*[33] Therefore, it's probably the main reason why CuS is not yet applied in electrochromic supercapacitors as TCEs.

As we known, making the continuous film into mesh structure with percolating random or periodic lines is an effective strategies to transform opaque or less transparent conductors to be much transparent, in which the frameworks can conduct current and leave large empty spaces that render the film transparent.[34,35] In this way, we can greatly increase the transparency of the TCEs without significantly reducing the electronic conductivity. Our group has recently reported a kind of CuS–nanosheet networks electrode with improved optoelectronic performance of 50 Ω sq^{-1} at 85% transmittance which was used as an efficient counter electrode for flexible quantum-dot solar cell.[36] However, due to the size of the spaces, those

[a]*Research Institute for Soft Matter and Biomimetics, Fujian Provincial Key Laboratory for Soft Functional Materials Research, College of Materials, Department of Physics, Xiamen University, Xiamen 361005, China. E-mail: wxguo@xmu.edu.cn*

[b]*Department of Physics, Faculty of Science, National University of Singapore, Singapore, 117542, Singapore. E-mail: phyliuxy@nus.edu.sg*

† Electronic supplementary information (ESI) available. See DOI: 10.1039/c7ra04476c

‡ Authors contributed equally to this work.

percolating electrodes cannot be regarded as continuous electrodes for some applications. By applying a graphene[37] or PEDOT:PSS[38] layer above, it is possible to make it a continuous conductive film. In addition, in the metal network electrodes, to some extent the covered PEDOT:PSS or graphene can protect the metal from oxidation. It is worth noting that besides optoelectronic performance, this design route is also beneficial for the mechanical stability of flexible and stretchable electrodes as a result of remarkable stress accommodation.

Here, we introduced a new kind of flexible TCE using CuS grids hybrid with graphene as conductive materials and PET as the supporting substrate. This graphene/CuS network (G–CuS) TCE was obtained by photolithography, chemical vapor deposition and a low temperature solvothermal reaction. It exhibits an R_s of ~20 Ω sq^{-1} at ~85% transmittance, which is superior to sputtered CuS films. In addition, the G–CuS TCE displays a remarkable mechanical flexibility and excellent chemical stability under bending stresses and polyaniline (PANI) electrodeposition in acid solution, respectively. Moreover, such symmetrical PANI supercapacitor can also act as a smart device for energy storage and its responsive color variation can simultaneously monitor the level of stored energy.

Experimental section

Materials

Ethanol (>99.7%), sulfuric acid (H_2SO_4, 95–98%) and polyvinyl alcohol (PVA-124) were purchased from Shantou Xilong chemical Co. Ltd. (Guangdong, China), and they were of analytical reagent grade (AR). Sublimed sulfur powders (AR, >99.5%) and aniline (ACS grade, >99.0%) were supplied from Aladdin Co. Ltd. (Shanghai, China). All chemicals were used as received without further purification. Deionized water was used throughout the electrochemical experiments. Ag target (99.99%) was purchased from Zhongnuoxincai (Beijing) Technology Co., Ltd.

Fabrication of various flexible transparent conducting electrodes (TCEs)

Ag networks were fabricated on PET substrates using electrospinning and sputtering methods as reported previously:[39] freestanding PVA fibers were spun on an aluminium frame to form a network and then a thin layer of Ag film with a thickness of 50–100 nm was deposited on the polymer fiber network by magnetron sputtering. The Ag network was derived after transferring the whole structure onto the PET substrate and removing the PVA networks. Graphene/Cu network films (G–Cu) with R_s of ~1 Ω sq^{-1} fabricated by photolithography and chemical vapor deposition (CVD) techniques were provided by Xiamen G-CVD Graphene Technology Co., Ltd. Then, the G–Cu films were converted into graphene/CuS network (G–CuS) TCEs by soaking them in sulfur ethanol solution (0.6 g L^{-1}) at 60 °C for 12–24 h.[40]

Electrodeposition of PANI

The deposition of PANI was performed using a CHI 660E electrochemical workstation in conventional three-electrode system

under a galvanostatic current density of 0.1 mA cm^{-2}. One of the various TCEs was used as working electrode, a Pt foil was used as counter electrode, and an Ag/AgCl electrode was used as reference electrode, respectively. An aqueous solution containing 0.2 M aniline monomer and 0.5 M H_2SO_4 was used as the electrolyte.

Assembly of a symmetrical supercapacitor

A symmetrical supercapacitor was fabricated with H_2SO_4–PVA hydrogel as the electrolyte.[17] The H_2SO_4–PVA hydrogel was mixed from PVA aqueous solution and H_2SO_4 with the PVA/H_2SO_4 mass ratio of 1/1. Specifically, 5 g PVA was added into 45 g DI water and heated to 85 °C for 4 h to get a clear solution. After cooling down to room temperature, 5 g H_2SO_4 aqueous solution (85 wt%) was added to the above solution under stirring for 30 min. The H_2SO_4–PVA hydrogel electrolyte was scrape-coated on the surface of the two symmetrical G–CuS electrodes (15 mm × 30 mm). Subsequently, these two electrodes were stacked face to face and the hydrogel electrolyte was used as both separator and electrolyte simultaneously. A conductive copper foil was then used to stick the edge of each electrode to form good electrical contact with an electrochemical instrument. Through this way, a symmetrical supercapacitor was attained.

Characterization

A four-point probe (RTS-8) was used to measure the films' R_s. The light transmittances of all the TCEs were measured by a UV-vis-NIR spectrophotometer (Perkin-Elmer Lambda 750). The morphology of the prepared materials were examined by a scanning electron microscopy (SEM, Hitachi SU-70) and a Leica microscope (DM 6000BDM 6000B). The components of G–Cu, G–CuS and G–CuS/PANI were investigated by Raman spectrometer (LabRAM HR Evolution). All electrochemical measurements were performed using a CHI660E in a conventional three-electrode system with the G–CuS/PANI, a Pt foil, an Ag/AgCl electrode, and 0.5 M H_2SO_4 aqueous solution as working electrode, counter electrode, reference electrode, and the electrolyte, respectively. Areal capacitance of supercapacitors is calculated according to the following eqn (1):

$$C = (I \times t)/(V \times S) \tag{1}$$

where C is areal capacitance (F cm^{-2}), I stands for the discharge current (mA), t is the discharge time (s), V represents the potential window (V), and S is the effective surface area of the active material electrode (cm^2).

Results and discussion

Morphology and component analysis

Fig. 1A schematically presents the processes of the synthesis of G–CuS/PANI on polyethylene terephthalate (PET) substrate through solvothermal reaction and electropolymerization. Firstly, Cu networks were converted into CuS networks by immersing G–Cu into an ethanol solution containing 0.6 g L^{-1}
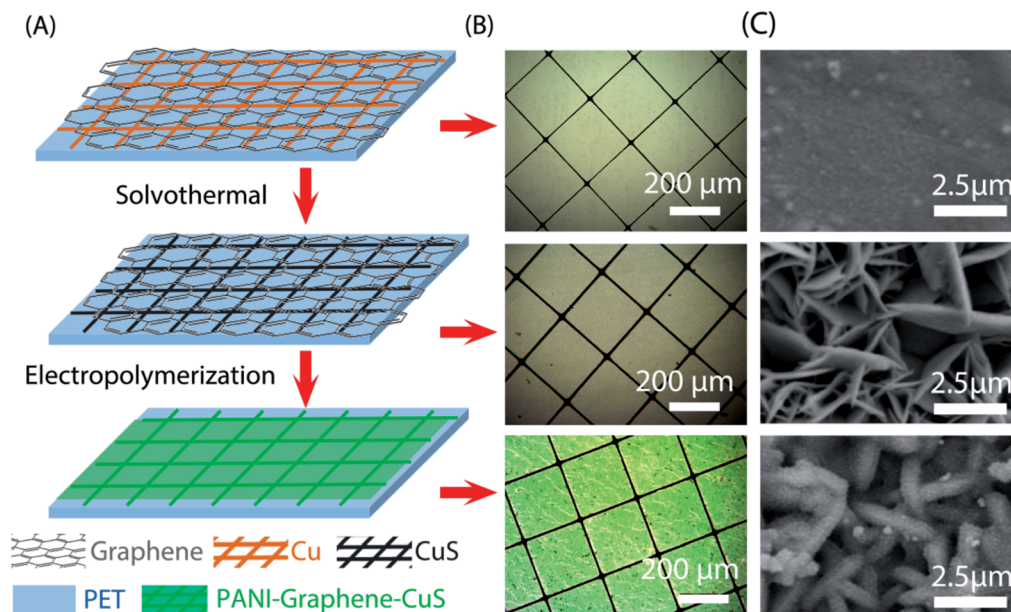
Fig. 1 (A) Schematic illustration of the processes of synthesizing G–CuS/PANI on the PET substrate through solvothermal and electro-polymerization reactions. The resulted optical (B) and SEM (C) images of the corresponding film are shown on the right two columns, respectively.

sulfur. By using this simple solvothermal method, we can easily obtain a large-scale flexible G–CuS TCE (Fig. S1 in the ESI†). It follows the microscope photographs in Fig. 1B that no obvious changes were observed in the morphology after the Cu networks were converted into CuS networks. The girds of the networks have a square configuration with the 300 μm length of the side (L) and the 10 μm width of the grid line (w). Corresponding SEM morphology images shown in Fig. 1C present that smooth Cu grid had been transformed into sheet-like CuS grid with the sheet thickness of ∼50 nm. Secondly, PANI was electro-deposited on G–CuS TCE by the electropolymerization method at a current density of 0.1 mA cm^{-2}. It follows the micrograph in Fig. 1B that the whole TCE was uniformly coated by a green film. The corresponding SEM images for the green film on grid line and empty area are displayed in Fig. 1C and 2C, respectively, indicating the whole TCE was uniformly coated by a layer of PANI nanorods arrays with a diameter of ∼50 nm.

The components of G–Cu, G–CuS and G–CuS/PANI were investigated by Raman analysis in Fig. 2A. The two typical peaks of graphene located at ∼1580 cm^{-1} and 2681 cm^{-1} can be readily indexed to the in-plane bond stretching motion of C sp^2 atoms (G band) and the inter-valley double resonance Raman scattering (G′ band), respectively.[41] In contrast to the G–Cu networks, the Raman spectrum of the CuS nanostructures showed a distinct band at 472 cm^{-1}, which originates from the lattice S–S stretching of covellite.[42] After deposition of PANI, several weak Raman peaks located at 414–580, 1322, 1490, and 1585 cm^{-1} emerged in the spectrum which are attributed to the out-of-plane C–N–C torsion, C–N$^+$ stretching, C=N stretching of quinoid, and C–C stretching of benzenoid in PANI, respectively. Furthermore, energy dispersive X-ray spectroscopy (EDS) spectrum of G–CuS/PANI is displayed in Fig. 2B. The weak peak

located at 0.38 eV is corresponding to the N element which belongs to PANI, which is consistent with the result of EDS mapping in Fig. 2D. Thanks to the wrapped graphene layer, PANI was not only polymerized on the surface of CuS grids, but also uniformly covered the entire G–CuS surface including the empty area as shown in Fig. 2D. On the contrary, PANI was only deposited on the CuS grids when we removed the wrapped graphene film (see Fig. S2 in the ESI†). The covered graphene plays an important role to increase the electronic distribution uniformity in the electrochemical polymerization process, and it is the PANI in the empty area that dominantly causes color changes of the supercapacitor.[38]

Physicochemical properties of TCEs

To investigate the physicochemical properties of the G–CuS network, three other TCEs including commercial ITO, G–Cu and Ag networks were introduced as references. Fig. 3A shows the photograph of the four different flexible TCEs, they were commercial ITO (13 Ω sq^{-1}), (∼1 Ω sq^{-1}), Ag network (5 Ω sq^{-1}), and G–CuS (20 Ω sq^{-1}), respectively. To examine the mechanical flexibility of the four TCEs, each sample with a size of 3.5 cm × 5 cm was bent to the radium of 0.5 cm, and then released to the initial position for 1000 times. As can be seen from Fig. 3B, negligible changes in the resistance were observed for G–Cu, Ag networks and G–CuS networks, while ITO suffered from serious damage and its R_s increased sharply. The broad transmittance spectra of the aforementioned four TCEs are plotted in Fig. 3C and D. The transmittances of the Ag network, G–Cu and G–CuS are almost flat in the range of 400–2000 nm while that of ITO demonstrated a sharp decrease in the range of wavelength greater than 700 nm, indicating network TCEs can solve the low
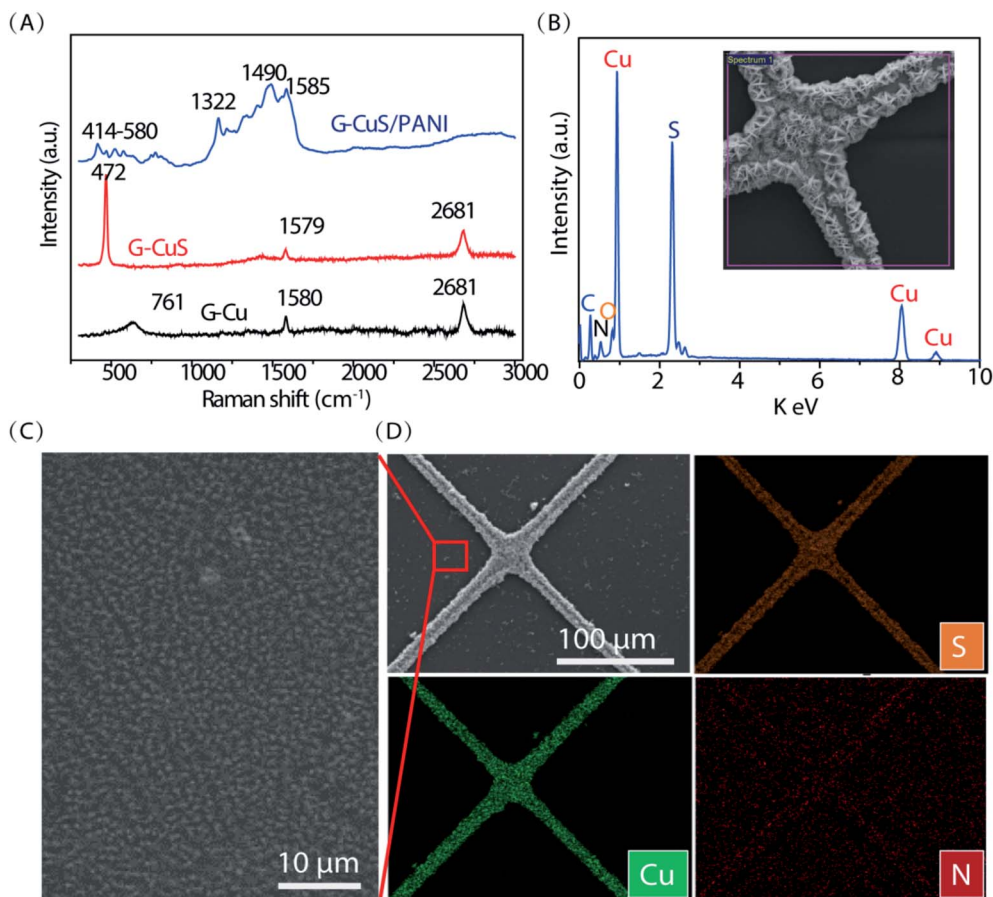
Fig. 2 (A) Raman spectra of G–Cu, G–CuS and G–CuS/PANI. (B) EDS spectrum of G–CuS/PANI. (C) SEM image of PANI grown on the G–CuS film (empty area of the grid frame). (D) EDS mapping of G–CuS/PANI demonstrates the successful fabrication of the CuS networks and the PANI film was uniformly distributed across the whole TCE.

infrared transmittance problem for the ITO films. Apart from high infrared transmittance, network TCEs exhibit excellent optoelectronic performance. The average transmittances of visible lights of Ag network (5 Ω sq^{-1}) and G–Cu (~1 Ω sq^{-1}) are about 88.3% and 88.1%, respectively, which are much better than that of ITO (13 Ω sq^{-1} at a maximum transmittance of 71%). According to the calculation from eqn (S1) and Fig. S3 in the ESI,† the optical transmittances of the network TCEs mainly depend upon the unpatterned area.[35] Therefore, in this work, the light transmittance of the Cu networks should be 93.4% according to the L and w of the grid are 300 μm and 10 μm, respectively. The transmittance of G–Gu TCE (88.1%) exhibited slightly lower than that of Cu networks (93.4%) can be attributed to the wrapped graphene layer reduced the light transmittance. It is worth to note that negligible decrease in transmittance was observed after converting G–Cu networks into G–CuS networks, indicating the transparency of the CuS film can be significantly increased after making the continuous film into mesh structure.

Chemical stability is another important feature for TCEs in ECDs. Fig. 3E shows chronopotentiometric curves obtained during the galvanostatic electropolymerization of PANI on the aforementioned four flexible TCEs in an aniline–H$_2$SO$_4$

aqueous solution. For G–CuS, it reached a maximum potential value of about 0.80 V in less than 80 s corresponding to the formation of PANI, then, the potential decreased slightly and remained stable when we further extending the polymerization time.[43] As for ITO, the potential remained stable in the first 880 s and then sharply increased due to ITO shows poor chemical stability and strong sensitivity to corrosive salts and acids.[44] For Ag network and G–Cu, the deposition potentials at the beginning were only 0.42 V and 0.12 V, which is attributed to their superior conductivity. However, their chemical stability was also poor and only remained stable for 20 s and 960 s, respectively. It should be noted that G–Cu exhibited higher chemical stability than Ag network due to the fact that the graphene can retard the metallic TCEs to some extent oxidation in erosion solution.[20,45,46] Fig. 3F shows the corresponding photograph before and after deposition of PANI film, indicating that PANI can be only deposited on G–CuS TCE while almost no PANI was observed on the other three TCEs. The clearer SEM images as shown in Fig. S4 (see ESI†) displays that both the Ag networks and Cu grids corroded and were eventually fractured. As we know, the major barrier to commercialization of most of the metallic TCE is their poor chemical stability. As for the CuS material, we has also previously demonstrated that CuS shows
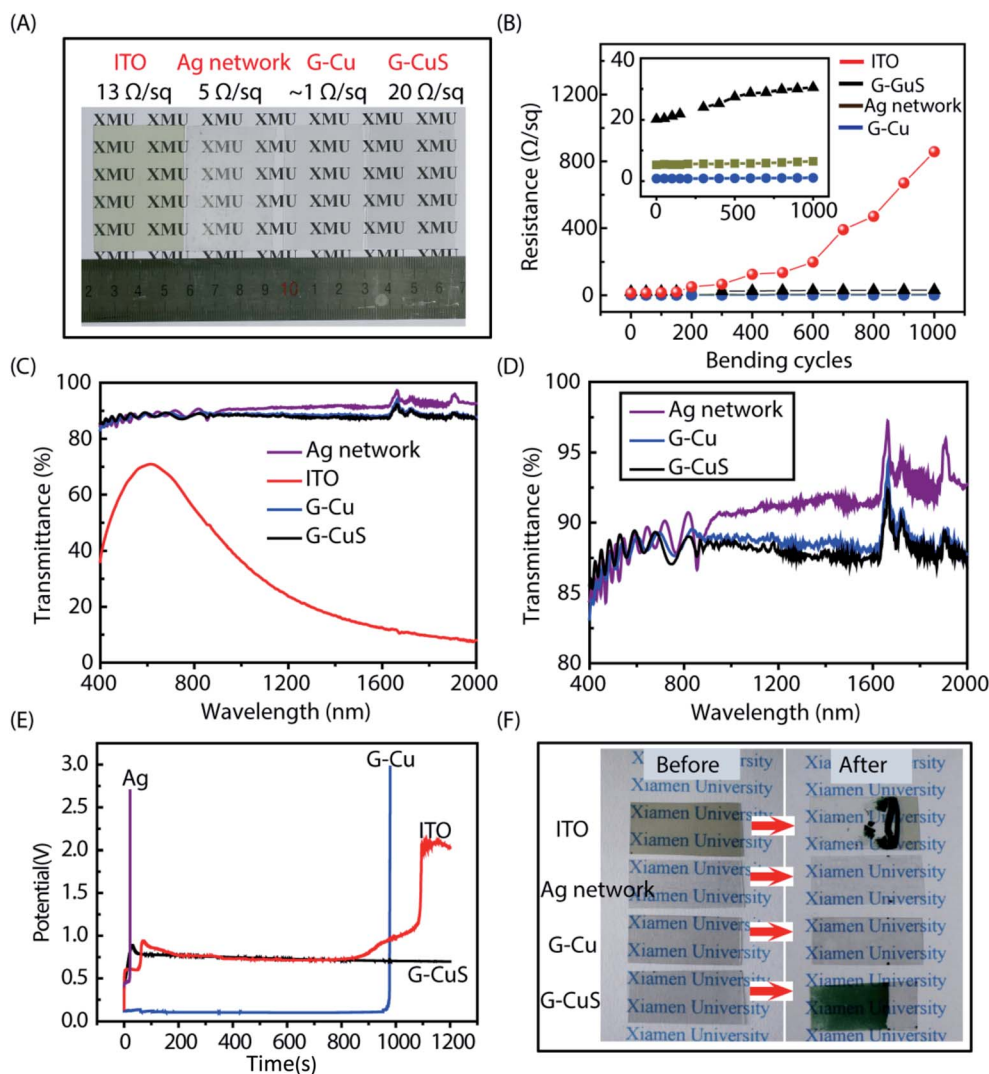
Fig. 3 (A) Photograph of the four different flexible TCEs, they are ITO, Ag networks, G–Cu and G–CuS, respectively. (B) Variations in R_s of the four different TCEs as a function of the number of bending cycles with the bending radius of 0.5 cm. (C and D) Visible-NIR transmittance spectra of the four different TCEs. (E) Electrodeposition curves of PANI grown onto the four different TCEs under a galvanostatic density of 0.1 mA cm^{-2} in 0.5 M H_2SO_4 aqueous solution containing 0.2 M aniline, and (F) their corresponding photos before and after electropolymerization.

excellent chemical stability when exposed to various conditions of thermal oxidation at 160 °C, humid air with 80% relative humidity at 85 °C, and H_2O_2 solution, respectively.[47] G–CuS TCEs represent a new opportunity for emerging flexible electronics required working in hash conditions.

Characterizations of electrochromic–supercapacitive performance

Based on the PANI electrodeposition results, we only chose G–CuS to further evaluate the possibility of its use as a TCE in the electrochromic supercapacitor. As we know, both electrochromic and supercapacitive behaviors of PANI are attributed to the redox reaction in the same acid electrolyte.[48] In this context, we can simultaneously develop a multifunctional electrochromic supercapacitor that is capable of energy storage and transmittance adjustment. To evaluate the performance of the

G–CuS/PANI film as an electrochromic-supercapacitor electrode, the charge–discharge curves at different current densities (Fig. 4A) and corresponding *in situ* transmittance at 620 nm (Fig. 4B) were tested. As can be seen from Fig. 4A, both the charging and discharging time increased while decreasing charge–discharge current densities from 0.050 mA cm^{-2} to 0.025 mA cm^{-2}. As shown in Fig. 4B, the coloring process resulted in decreasing the transmittance while the bleaching process was just the reverse. According to the Fig. 4A and B, the variation of area capacitance (C) and optical modulation (ΔT) as function of current densities can be calculated and corresponding curves were displayed in Fig. 4C. It is obvious that C and ΔT decreased gradually with increasing the current density. It could be attributed the fact that the migration of the electroactive ions is limited to access inner surface of the active material for energy storage owing to the diffusion effect at high current density.[38] It follows from Fig. 4C that G–CuS/PANI
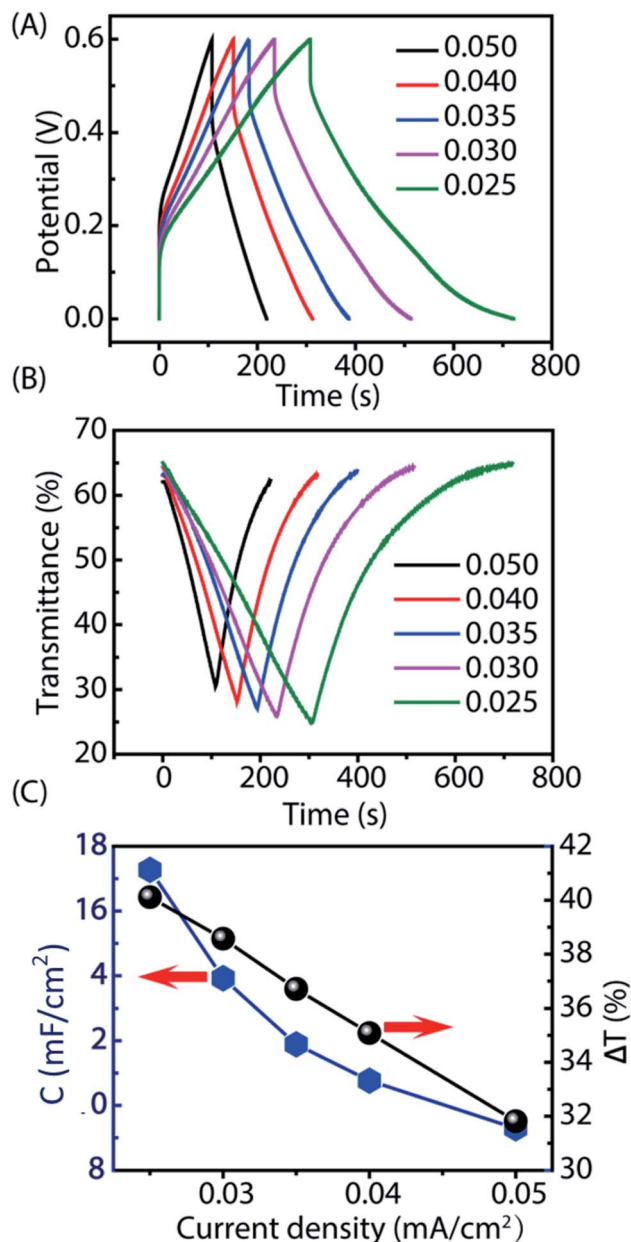
Fig. 4 Galvanostatic charge–discharge curves (A) in the potential range of 0 to 0.6 V and corresponding *in situ* optical responses (B) measured at 620 nm under different current densities for the G–CuS/PANI film. (C) The dependence of area capacitance and ΔT on the current density.

exhibited area capacitances of 17.3, 13.9, 11.9, 10.8 and 9.3 mF cm^{-2} at 0.025, 0.030, 0.035, 0.040 and 0.050 mA cm^{-2}, along with optical modulation of 40.1%, 38.6%, 36.7%, 35.1% and 31.8%, respectively. In addition, C and ΔT at a high current density of 0.050 mA cm^{-2} sustained 54% and 79%, respectively, compared to the values at a low current density of 0.025 mA cm^{-2}. The supercapacitive results of our work is comparable to that with the PEDOT/PET as the transparent conductive electrode, which is from 6 to 15 mF cm^{-2} when at the current density from 0.3 to 0.01 mA cm^{-2}.[17] And after galvanostatic charge–discharge tests for 200 cycles at a current density of
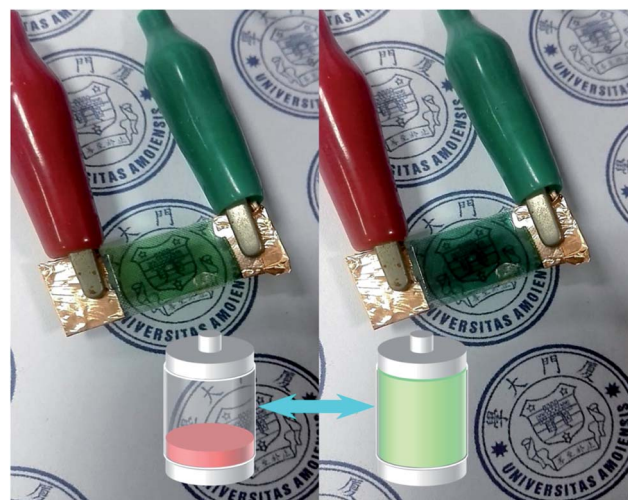

Fig. 5 The color change of a supercapacitor responds to the level of stored energy during the charge–discharge process (a related movie has been provided in ESI,† Movie S1).

0.045 mA cm^{-2} as shown in Fig. S5 in the ESI,† G–CuS/PANI displayed a favorable cyclic stability with a decay of only 24% compared to its initial area capacitance. Furthermore, the corresponding *IR* drops at different current densities were displayed in Fig. S6 in the ESI.† The *IR* drop is generally attributed to the charge–discharge current density besides the electrolyte potential drop and contact resistance.[17] G–CuS/PANI showed low *IR* drops from 76.73 mV at 0.025 mA cm^{-2} to 148.87 mV at 0.050 mA cm^{-2}. The aforementioned results demonstrate that the G–CuS/PANI electrode exhibited a supercapacitive performance and an exciting combination of the electrochromic and supercapacitive properties. Furthermore, we assembled a symmetrical supercapacitor with H_2SO_4–PVA hydrogel as the electrolyte, which presented a excellent electrochromic response to the galvanostatic charge–discharge process as shown in Fig. 5. Its noticeable color variation enables users to intuitively evaluate the level of stored energy by naked eyes in a predictable manner.

Conclusions

In summary, a newly designed G–CuS TCE with high transparency, flexibility and conductivity has been fabricated by photolithography, chemical vapor deposition and a low-temperature solvothermal reaction. This novel TCE achieves an R_s of ~20 Ω sq^{-1} with a transmittance of over 85%. During the bending test, G–CuS exhibited remarkable mechanical stability with a small R_s increase of ~10 Ω sq^{-1} after 1000 bending cycles. Uniform PANI was successfully deposited on the G–CuS film by the galvanostatic electrodeposition in aniline–H_2SO_4 solution. The PANI/G–CuS electrode exhibited an excellent electrochromic supercapacitive performance, which achieved an area capacitance of 17.3 mF cm^{-2} along with a large optical modulation of 40.1%. Furthermore, a symmetrical supercapacitor was assembled in which the electrochromic property can intuitively reflect the condition of energy storage

for visual assessment. The G–CuS TCE with excellent conductivity, transparency, mechanical stability and chemical stability will have a promising future in the flexible electronics. This work may supply an inspiration to the design of TCEs for electrochromic supercapacitors.

Acknowledgements

References

1 M. Salanne, B. Rotenberg, K. Naoi, K. Kaneko, P. L. Taberna, C. P. Grey, B. Dunn and P. Simon, *Nat. Energy*, 2016, **1**, 16070.

2 W. Li, J. Liu and D. Zhao, *Nat. Rev. Mater.*, 2016, **1**, 16023.

3 P. Simon and Y. Gogotsi, *Nat. Mater.*, 2008, **7**, 845–854.

4 P. Yang, P. Sun and W. Mai, *Mater. Today*, 2015, **19**, 394–402.

5 G. Cai, X. Wang, M. Cui, P. Darmawan, J. Wang, A. L.-S. Eh and P. S. Lee, *Nano Energy*, 2015, **12**, 258–267.

6 Y. Tian, S. Cong, W. Su, H. Chen, Q. Li, F. Geng and Z. Zhao, *Nano Lett.*, 2014, **14**, 2150–2156.

7 D. Wei, M. R. Scherer, C. Bower, P. Andrew, T. Ryhänen and U. Steiner, *Nano Lett.*, 2012, **12**, 1857–1862.

8 X. Chen, H. Lin, P. Chen, G. Guan, J. Deng and H. Peng, *Adv. Mater.*, 2014, **26**, 4444–4449.

9 X. Chen, H. Lin, J. Deng, Y. Zhang, X. Sun, P. Chen, X. Fang, Z. Zhang, G. Guan and H. Peng, *Adv. Mater.*, 2014, **26**, 8126–8132.

10 W. Liu, M. S. Song, B. Kong and Y. Cui, *Adv. Mater.*, 2017, **29**, 1603436.

11 M. Nikolou, A. L. Dyer, T. T. Steckler, E. P. Donoghue, Z. Wu, N. C. Heston, A. G. Rinzler, D. B. Tanner and J. R. Reynolds, *Chem. Mater.*, 2009, **21**, 5539–5547.

12 L. Hu, G. Gruner, D. Li, R. B. Kaner and J. Cech, *J. Appl. Phys.*, 2007, **101**, 016102.

13 J. H. Lee, D. W. Shin, V. G. Makotchenko, A. S. Nazarov, V. E. Fedorov, Y. H. Kim, J.-Y. Choi, J. M. Kim and J.-B. Yoo, *Adv. Mater.*, 2009, **21**, 4383–4387.

14 W. R. Lian, Y. C. Huang, Y. A. Liao, K. L. Wang, L. J. Li, C. Y. Su, D. J. Liaw, K. R. Lee and J. Y. Lai, *Macromolecules*, 2011, **44**, 9550–9555.

15 C. Sachse, N. Weiß, N. Gaponik, L. Müller-Meskamp, A. Eychmüller and K. Leo, *Adv. Energy Mater.*, 2014, **4**, 1300737.

16 C. Lee, C. Kim, M. Jeong, J. Kim, J. Lee, J. W. Oh, J. Lee, S. H. Kim, S. S. Park and J. M. Kim, *RSC Adv.*, 2015, **5**, 77288–77295.

17 K. Wang, H. Wu, Y. Meng, Y. Zhang and Z. Wei, *Energy Environ. Sci.*, 2012, **5**, 8384–8389.

18 K. Sanglee, S. Chuangchote, P. Chaiwiwatworakul and P. Kumnorkaew, *J. Nanomater.*, 2017, **2017**, 8.

19 B. W. An, B. G. Hyun, S.-Y. Kim, M. Kim, M.-S. Lee, K. Lee, J. B. Koo, H. Y. Chu, B.-S. Bae and J.-U. Park, *Nano Lett.*, 2014, **14**, 6322–6328.

20 Y. Ahn, Y. Jeong, D. Lee and Y. Lee, *ACS Nano*, 2015, **9**, 3125–3133.

21 Y. H. Kim, L. Müller-Meskamp and K. Leo, *Adv. Energy Mater.*, 2015, **5**, 1401822.

22 S. K. Balasingam, M. Lee, B. H. Kim, J. S. Lee and Y. Jun, *Dalton Trans.*, 2017, **46**, 2122–2128.

23 X. Li, W. Li, M. Li, P. Cui, D. Chen, T. Gengenbach, L. Chu, H. Liu and G. Song, *J. Mater. Chem. A*, 2015, **3**, 2762–2769.

24 B. M. Gray, A. L. Hector, M. Jura, J. R. Owen and J. Whittam, *J. Mater. Chem. A*, 2017, **5**, 4550–4559.

25 W. Li, C. Y. Cao, C. Q. Chen, Y. Zhao, W. G. Song and L. Jiang, *Chem. Commun.*, 2011, **47**, 3619–3621.

26 W. Li, X. Gao, D. Xiong, F. Xia, J. Liu, W. G. Song, J. Xu, S. M. Thalluri, M. F. Cerqueira, X. Fu and L. Liu, *Chem. Sci.*, 2017, **8**, 2952–2958.

27 Z. Zhang, S. Liu, J. Xiao and S. Wang, *J. Mater. Chem. A*, 2016, **4**, 9691–9699.

28 W. Li, X. Gao, X. Wang, D. Xiong, P.-P. Huang, W.-G. Song, X. Bao and L. Liu, *J. Power Sources*, 2016, **330**, 156–166.

29 A. Cuevas, R. Romero, D. Leinen, E. A. Dalchiele, J. R. Ramos-Barrado and F. Martin, *Sol. Energy Mater. Sol. Cells*, 2015, **134**, 199–208.

30 S. V. Bagul, S. D. Chavhan and R. Sharma, *J. Phys. Chem. Solids*, 2007, **68**, 1623–1629.

31 P. Parreira, G. Lavareda, J. Valente, F. T. Nunes, A. Amaral and C. N. de Carvalho, *Phys. Status Solidi A*, 2010, **207**, 1652–1654.

32 P. Parreira, G. Lavareda, A. Amaral, A. M. Botelho do Rego, O. Conde, J. Valente, F. Nunes and C. Nunes de Carvalho, *J. Alloys Compd.*, 2011, **509**, 5099–5104.

33 K. D. Yuan, J. J. Wu, M. L. Liu, L. L. Zhang, F. F. Xu, L. D. Chen and F. Q. Huang, *Appl. Phys. Lett.*, 2008, **93**, 132106.

34 N. Fukaya, D. Y. Kim, S. Kishimoto, S. Noda and Y. Ohno, *ACS Nano*, 2014, **8**, 3285–3293.

35 B. Y. Ahn, D. J. Lorang and J. A. Lewis, *Nanoscale*, 2011, **3**, 2700–2702.

36 Z. Xu, T. Li, F. Zhang, X. Hong, S. Xie, M. Ye, W. Guo and X. Liu, *Nanoscale*, 2017, **9**, 3826–3833.

37 Y. Zhu, Z. Sun, Z. Yan, Z. Jin and J. M. Tour, *ACS Nano*, 2011, **5**, 6472–6479.

38 G. Cai, P. Darmawan, M. Cui, J. Wang, J. Chen, S. Magdassi and P. S. Lee, *Adv. Energy Mater.*, 2016, **6**, 1501882.

39 X. M. Wu, W. Z. Zhang, Q. G. Wang, Y. Wang, H. Y. Yan and W. X. Chen, *Synth. Met.*, 2016, **212**, 1–11.

40 W. Ke, G. Fang, H. Lei, P. Qin, H. Tao, W. Zeng, J. Wang and X. Zhao, *J. Power Sources*, 2014, **248**, 809–815.

41 L. M. Malard, M. A. Pimenta, G. Dresselhaus and M. S. Dresselhaus, *Phys. Rep.*, 2009, **473**, 51–87.

42 Y. Du, Z. Yin, J. Zhu, X. Huang, X.-J. Wu, Z. Zeng, Q. Yan and H. Zhang, *Nat. Commun.*, 2012, **3**, 1177.

43 J. Yang and D. C. Martin, *Sens. Actuators, B*, 2004, **101**, 133–142.

44 S. W. Gaarenstroom, M. P. Balogh, M. C. Militello, R. A. Waldo, C. A. Wong, N. A. Kelly, T. L. Gibson and M. D. Kundrat, *Surf. Interface Anal.*, 2005, **37**, 385–392.

45 W. Wu, N. G. Tassi, D. J. Walls, L. Zhang and B. Willner, *Appl. Phys. Lett.*, 2014, **105**, 223104.

46 R. Mehta, S. Chugh and Z. Chen, *Nano Lett.*, 2015, **15**, 2024–2030.

47 X. Zhang, W. Guo, G. Gao, M. Que, C. Pan and Z. L. Wang, *J. Mater. Chem. C*, 2016, **4**, 4733–4739.

48 X. Xiang, W. Zhang, Z. Yang, Y. Zhang, H. Zhang, H. Zhang, H. Guo, X. Zhang and Q. Li, *RSC Adv.*, 2016, **6**, 24946–24951.